Check for updates

Influences of atmospheric blocking on North American summer heatwaves in a changing climate: a comparison of two Canadian Earth system model large ensembles

Dae Il Jeong[1] · Alex J. Cannon[2] · Bin Yu[1]

Abstract

As summer heatwaves have severe adverse impacts on human society and ecosystems, there is need to better understand their meteorological drivers and future projections under climate change. This study investigates the linkage between atmospheric blocking and summer (June–August) heatwaves over North America using two reanalysis datasets (ERA-Interim and NCEP-DOE-R2) and two large-ensembles of Canadian Earth System Models (CanESM2 and CanESM5) for the 1981–2010 baseline period as well as projected changes under high-emission scenarios out to 2071–2100. Compared to NCEP-DOE-R2, both ensembles underestimate summer blocking frequency in the north Pacific, Alaska, and western Canada (by − 37%), while CanESM2 ensemble also underestimates blocking frequency in central and eastern Canada (by − 36%). CanESM5 generally shows better performance than CanESM2 in its reproduction of blocking frequency over central and eastern Canada, which is consistent with its overall improvements in simulating large-scale climate patterns. The two ensembles, however, agree with the reanalyses in their blocking-heatwave linkages. Above-normal heatwave frequency occurs in the blocking core and its surroundings due to positive heat flux anomalies, while below-normal frequency occurs at remote locations on the eastern and/or southern flanks of the blocking core due to cold air temperature advection anomalies. Future projections in central Canada differ between the models, largely due to the significant under-representation of blocking frequency by CanESM2. However, the two ensembles generally project similar behavior between the baseline and future period for spatial distributions of blocking-heatwave linkages, indicating blocking will continue to play an important role in the development of summer heatwaves in the future.

✉ Dae Il Jeong
jeong.daeil@ec.gc.ca

1 Climate Research Division, Environment and Climate Change Canada, Toronto, ON M3H 5T4, Canada

2 Climate Research Division, Environment and Climate Change Canada, Victoria, BC V8W 2Y2, Canada

1 Introduction

Summer heatwaves have received intensive attention over the past decades due to their severe adverse impacts on human society and ecosystems. The European summer heatwave in 2003 was responsible for more than 35,000 deaths and economic losses of 10 billion USD (Fischer et al. 2007). This event also led to forest fires in Portugal and associated severe damages to ecosystems with economic losses of more than 1 billion Euros (García-Herrera et al 2010). The USA summer heatwave in 1988 resulted in 5000–10,000 deaths (National Climatic Data Center 2001). An estimated 840 deaths of Canada and the USA resulted by the direct consequences of the Western North America heatwave in 2021 (Overland 2021). Heatwaves also have negative effects on crops, livestock, and milk production (Sejian et al. 2012). Meanwhile, the frequency of heatwaves has increased in large parts of Europe and Asia since the middle of the twentieth century (Seneviratne et al. 2021). Peterson et al. (2013) reported the highest and second highest number of heatwaves occurred in the 1930s and 2000s decades in the USA; however, a higher number of heatwaves in the 2010s than in the 2000s were reported (Alizadeh et al. 2022). Anthropogenic global warming is blamed for increased probability of heatwave occurrences (e.g., Fischer and Knutti 2015; Seneviratne et al. 2021). Moreover, projections from multi-model ensembles of global climate models (GCMs) suggest that heatwaves will be more intense, more frequent, and last longer over most land areas in future warming climates (e.g., Fischer and Knutti 2015; Dosio et al. 2018). Therefore, it is important to understand the mechanisms driving heat extremes and how these mechanisms and extremes will be affected by climate change.

Heatwaves occurring in mid- to high-latitudes are often associated with atmospheric blocking events, which are originally defined as quasi-stationary anti-cyclonic circulation anomalies that interrupt the predominant westerly flow and persist for several days (Trigo et al. 2004), but they are also associated with persistent or unusual features in storm tracks (Zappa et al. 2014). Atmospheric blocking drives above-normal temperature anomalies for several days based on the combination of radiative heating under clear-sky conditions and warm air advection driven by clockwise anti-cyclonic circulations, dependent on the flow patterns and position of blocking and its features at the seasonal scale (Pfahl and Wernli 2012; Schaller et al. 2018). Besides this, heatwaves can be amplified by land–atmosphere feedbacks in transitional climate regions based on reduction in evaporative cooling with enhanced persistence driven by soil moisture memory. Drought conditions are also a triggering factor that can exacerbate surface and low-level air temperature from an increase in surface sensible heat flux during drying persistent conditions (Black et al. 2004).

GCMs are the most widely used tools for simulating the historical climate, with observed greenhouse gas concentrations and radiative forcing, as well as for making projections of future climates under different anthropogenic forcing scenarios on a global scale. Ideally, GCMs should properly replicate atmospheric circulation features on various spatiotemporal scales. In particular, the linkage between blocking and heatwaves is an important synoptic-scale feature of the climate system that should be replicated by GCMs for current risk management and future adaptation strategies. However, GCMs generally show biased atmospheric circulation features due to coarse-scale resolution, missing orographic drag, sea surface temperature bias, etc. which affect the simulated blocking features; thus, underestimation of blocking frequency is a longstanding challenge (Anstey et al. 2013; Berckmans et al. 2013; Pithan et al. 2016; Davini and D'Andrea 2020). According to GCMs that contributed to the Coupled Model Intercomparison Project Phase 5 (CMIP5)

(Taylor et al. 2012), blocking frequency is underestimated in the Atlantic-European sector by around 10–30% in summer, with smaller negative biases in the Pacific-North American sector (Woollings et al. 2018). Underestimation of summer blocking frequency is also reported in CMIP Phase 6 (CMIP6) GCMs (Eyring et al. 2016), although they show an improvement in representing blocking frequency and persistence in the Atlantic and Pacific compared to CMIP5 (Davini and D'Andrea 2020; Schiemann et al. 2020). Meanwhile, CMIP5 and CMIP6 GCMs project decreases in future blocking frequency in mid-latitudes but increases in high-latitudes in summer due to the poleward shift in blocking activity with global warming (Woollings et al. 2018; Davini and D'Andrea 2020). The changed summer blocking frequency in a future climate could result in a change in summer heatwaves; however, changes in the background state or local feedbacks could counteract this linkage (Seneviratne et al. 2010; Woollings et al. 2018).

Connections between blocking and summer heatwaves have been studied over Atlantic-European sector. In particular, influences of blocking on individual mega-heatwave events that occurred over northern Europe and western Russia in 2003 (Fischer et al. 2007) and 2018 (Li et al. 2020) were investigated based on historical reanalysis datasets. Climatological blocking-heatwave linkages for historical and future simulations were also investigated using ensembles of GCMs. For instance, Brunner et al. (2018) found that Canadian Earth System Model version 2 (CanESM2) (Arora et al. 2011) reproduces observed blocking-heatwave linkages in simulations for summer over the 1981–2010 historical period; blocking significantly increases heatwave frequency in northern Europe, and the historical blocking-heatwave connection is maintained into the future (2070–2099). Similarly, Schaller et al. (2018) reported that (1) there is a significant correlation between blocking and summer heatwave magnitudes in northern Europe and western Russia for 1979–2015, (2) large ensembles of three GCMs (i.e., CanESM2, CESM-CAM4, CESM-CAM5) are able to reproduce that connection, and (3) the connection will not change in the future (2070–2099). However, blocking-heatwave connections and abilities of GCMs to reproduce these connections are rarely studied over the Pacific-North America region from either a historical or future climate change perspective. In an analysis of the National Centers for Environmental Prediction-National Center for Atmospheric Research (NCEP-NCAR) reanalysis dataset, Dong et al. (2018) found that a blocking event that persisted over the USA during August 2007 led to a record-breaking heatwave over southeastern USA. Although, changes in summer blocking intensity and persistence in the future have been investigated (Lee et al. 2021), their potential implications for future hot temperature extremes are not well documented over North America.

Here, we investigate observed linkages between blocking and summer (June–August) heatwaves over North America — with an emphasis on the Pacific-North America region — using two reanalysis datasets (ERA-Interim (Dee et al. 2011) and NCEP-Department of Energy reanalysis 2 (NCEP-DOE-R2) (Kanamitsu et al. 2002)) for the 1981–2010 baseline period. Subsequently, we evaluate two generations of Canadian Earth System Models (CanESM2 and CanESM version 5, CanESM5) for their ability to reproduce the observed blocking-heatwave connections. We also investigate projected changes in summer blocking activity and implications of these changes on heatwaves by the end of twenty-first century under high-emission scenarios (Representative Concentration Pathway RCP 8.5 (Moss et al. 2010) in CanESM2 and Shared Socioeconomic Pathway SSP5 8.5 (O'Neill et al. 2014) in CanESM5). Other atmospheric circulation and surface variables related to the blocking-heatwave linkage including anomalies of air temperature advection at 850 hPa, surface heat flux forcing, 1000–500 hPa geopotential thickness, and surface precipitation during blocking episodes are analyzed in the baseline and future periods. Note that this

is a complement study to the previous work conducted by Jeong et al. (2021) for the linkage between atmospheric blocking and winter cold spells over the Pacific-North American sector.

2 Data and Methods

2.1 Data

CanESM2 and CanESM5 are Earth System Models (ESMs) developed by the Canadian Centre for Climate Modelling and Analysis (CCCma) of Environment and Climate Change Canada (ECCC). Simulations from CanESM2 contributed to CMIP5 and those from CanESM5 contributed to CMIP6. CanESM2 is a comprehensive ESM that includes coupled atmosphere, ocean, sea-ice, land, and terrestrial and ocean carbon cycle components (Arora et al. 2011). Major improvements in CanESM5 from CanESM2 are incremental updates to the atmosphere, land-surface, and terrestrial ecosystem models, with the implementation of completely new components for the ocean, sea-ice, and marine ecosystems, as well as a new coupler (Swart et al. 2019). Virgin et al. (2021) provided further comparisons between the two versions in term of underlying causes of the difference in effective climate sensitivity.

This study makes use of variables from the two models, including daily maximum air temperature at 2 m and daily mean values of geopotential heights at 500, 850, and 1000 hPa, U and V components of wind at 850 hPa, surface precipitation, shortwave and longwave solar radiations (downward), and surface sensible and latent heat fluxes (upward). These variables are obtained from a 50-member ensemble of CanESM2 initial-condition simulations under historical (1981–2005) and RCP 8.5 (2006–2100) scenarios and a 20-member ensemble of CanESM5 initial-condition simulations under historical (1981–2014) and SSP5 8.5 (2015–2100) scenarios. Members of each CanESM ensemble share the same historical and future external forcings, differing only in initial conditions of the atmosphere and ocean state at the beginning of the simulation (i.e., 1950 for CanESM2 and 1850 for CanESM5). Consequently, members of each CanESM ensemble have different realizations of internal-variability under the given external forcings (Fyfe et al. 2017). RCP 8.5 and SSP5 8.5 are high emission (no mitigation policy) scenarios used for the CMIP5 and CMIP6, respectively, with a radiative forcing of 8.5 W/m^2 and roughly 5 °C increase in global mean temperature by the end of the twenty-first century compared to the pre-industrial level (IPCC 2013; Lee et al. 2021).

Both CanESM2 and CanESM5 use the spectral transform method for the atmosphere component with about 2.8° latitude × 2.8° longitude horizontal resolution (Arora et al. 2011; Swart et al. 2019). For this assessment, all variables are interpolated to a grid spacing of 2.5° × 2.5° using the first order conservative remapping method (Schulzweida 2019). The two large-ensembles are evaluated in their ability to reproduce observed blocking activity (based on NCEP-DOE-R2 and ERA-Interim reanalyses) and the linkage between blocking and summer heatwaves over Pacific-North America for the 1981–2010 baseline period. NCEP-DOE-R2 provides pressure level variables on a 2.5° grid but the other variables on a 1.9° grid; the latter are interpolated to 2.5° × 2.5° in this study. All variables of ERA-Interim are available at a horizontal-resolution of 0.75°, which are used without further treatment. Reanalysis datasets at higher resolutions (e.g., ERA5 at 0.28° resolution (Hersbach et al. (2020)) are not considered in this study. Rohrer et al. (2020) showed that

blocking characteristics are very similar (<3% difference) in ERA5 and its predecessor ERA-interim; however, coarse-resolution climate models cannot represent orography that is known to strongly affect the atmospheric circulation (Pithan et al. 2016). Meanwhile, the difference in resolutions of the reanalyses could be sensitive to detection methods of blocking events (Rohrer et al. 2020).

2.2 Blocking and associated anomalous atmosphere circulation and surface variables

Blocking indices could be categorized into three types, using absolute field (Davini et al. 2012), anomaly field (Schwierz et al. 2004), and combination of the two (Barriopedro et al. 2010). Woollings et al. (2018) compared summer blocking frequency diagnosed by the three types for 1958–2012 using three reanalysis datasets. All types display similar spatial pattern of the frequency over the Pacific-North American sector with more frequent blocking over the North Pacific than North American continent (Fig. 2 of Woollings et al. (2018)).

To identify the occurrence of blocking episodes, we apply a 2-dimensional absolute blocking detection method to meridional gradients of daily 500-hPa geopotential height fields (Z500) (Brunner et al. 2018; Woollings et al. 2018). For a given latitude ϕ, gradients of Z500 to the north (GZ500N) and to the south (GZ500S) are calculated along longitude λ

$$GZ500N(\lambda, \phi) = \frac{Z500(\lambda, \phi + \Delta\phi) - Z500(\lambda, \phi)}{\Delta\phi}$$

$$GZ500S(\lambda, \phi) = \frac{Z500(\lambda, \phi) - Z500(\lambda, \phi - \Delta\phi)}{\Delta\phi} \tag{1}$$

for $50°N \leq \phi \leq 75°N$ and $\Delta\phi = 15°$ latitude, thus focusing on high latitude blocking that diverts the main westerly flow (Davini et al. 2012). While, blocking activities based on ridge anomalies of cut-off lows or low latitude (40–50°N) blocking activities generated by fluctuations of the subtropical high pressure systems are not considered (Barriopedro et al. 2010). Instantaneous blocking (IB) is detected at the grid point (λ, ϕ) when gradients to the south and north simultaneously satisfy GZ500N < − 10 gpm/° and GZ500S > 0 gpm/°. Blocking events are then defined based on the 2-dimensional IB field by further taking into consideration spatial extent and temporal persistence. A spatial event is detected when IB conditions extend over at least 15° longitude while allowing for meridional movement within ± 5° of latitude. A blocking episode is then detected when a spatial IB event persists within 10° longitude for at least five consecutive days.

Blocking events are further detected over four different blocking regions (BRs) to explore both remote and coincident relationships between blocking and North American summer heatwaves. The four blocking regions are referred to as BR1 (180–150°W; north Pacific and western Alaska), BR2 (150–120°W; eastern Alaska and western Canada), BR3 (120–90°W; central Canada), and BR4 (90–60°W; eastern Canada). A blocking day in a blocking region occurs when more than half of the blocking region (i.e., 15° longitude in the region) is covered by a blocking event; thus, any two blocking regions could have the same blocking day when a blocking event is larger than 30° longitude. Wazneh et al. (2021) showed that the mean extension of blocking events in summer is about 22°.

Blocking days in the blocking regions are identified for each 30-year future period, incremented by 10 years, from the baseline to 2071–2100.

Atmosphere circulation and surface variables, including temperature advection at 850 hPa level (this level is selected to avoid noises stemming from surface boundary conditions such as topography, vegetation, roughness length, and land–atmosphere coupling), surface heat fluxes, surface precipitation, and 1000–500 hPa geopotential thickness, can influence extreme hot temperatures at the surface; therefore, anomalous behaviors of these variables during blocking are investigated to better understand the physical mechanisms behind the blocking-heatwave linkage. Anomalies of horizontal temperature advection (850 hPa) driven by anomalous wind flows during blocking are estimated using $-\frac{\partial \overline{T}}{\partial x} u' - \frac{\partial \overline{T}}{\partial y} v'$ (Lehtonen and Karpechko 2016), where $\overline{T}$ represents the climatological mean temperature in summer for the baseline or 2071–2100 periods, and u' and v' are the anomalous zonal and meridional wind components during blocks, relative to climatological means (i.e., Julian climatological values for the baseline or 2071–2100 periods). Net surface radiative and turbulent heat fluxes are estimated on a daily timescale via $R_S + R_L - LE - H$ (Pettenuzzo et al. 2010), where the components represent daily mean values of shortwave and longwave solar radiation (downward) and surface latent and sensible heat fluxes (upward), respectively. Consequently, the net heat flux roughly indicates the summation of the surface heat flux and total heat energy stored in the surface layer for a day when assuming the heat flux conduction from the soil is negligible. Anomalies of the surface heat fluxes during blocking days are calculated relative to climatological means for each baseline and future period. In the same way, anomalies of surface precipitation and 1000–500 hPa geopotential thickness during blocking days are calculated for the baseline and future periods.

2.3 Summer heatwaves

A summer heatwave is defined as a prolonged period of at least three consecutive hot days with daily maximum temperature above a threshold. The threshold used in this study is the 90th percentile of daily maximum temperatures in a 31-day window centered on a calendar day calculated for each ensemble member; heatwaves are estimated at each grid point on each calendar day for a given 30-year period (Pereira et al. 2017). Future heatwaves are defined in two different ways using two different thresholds for hot days: time-invariant (stationary) threshold calculated from the baseline period and time-variant (nonstationary) thresholds calculated for 30-year future periods from the baseline to 2071–2100. However, blocking-heatwave linkages are mainly investigated using the nonstationary hot day threshold, as the linkages are difficult to measure with the stationary definition due to the significant increase in the number and duration of heatwaves in a warming climate.

The strength of the blocking-heatwave connection is defined between each blocking region from BR1 to BR4 and each grid point over North America using the heatwave frequency anomaly $P_{ano} = (N_{HW|B}/N_B)/(N_{HW}/N)$ (Brunner et al. 2018), where N, N_{HW}, N_B, and $N_{HW|B}$ represent total number of summer days, number of heatwave days, number of blocking days, and number of heatwave days during blocking for a 30-year period. Thus, this anomaly represents the ratio of the conditional probability of heatwave days during blocking episodes to the unconditional (climatological) probability of heatwave days. The anomaly is larger than one when the conditional occurrence probability of heatwaves is higher than the unconditional occurrence probability, and close to one when blocking is not associated with heatwaves.

Statistical significance of the heatwave frequency anomaly is detected in each ensemble member using a block bootstrap resampling approach that accounts for the complicated spatiotemporal correlation structure of dataset (Efron and Tibshirani 1994). Autocorrelation in blocking and heatwaves is preserved using contiguous 15-day bootstrap resamples that could include a long blocking episode as well as a heatwave. The resampling is repeated 100 times from the series of daily blocking in each blocking region and heatwaves at each North American grid point. Statistical significance is defined when the 5th–95th percentile range, as quantified by the bootstrap, excludes one. The anomaly is either statistically significantly higher than climatology when the 5th percentile is larger than one, or lower when the 95th percentile is smaller than one. Anomalies of surface heat fluxes and 1000–500 hPa geopotential thickness are also tested their statistical significance using the bootstrap resampling approach. Four sub-regions of North America are defined as northwest (NW; 170–102°W and 50–70°N), northeast (NE; 102–52°W and 50–70°N), southwest (SW; 140–102°W and 30–50°N), and southeast (SE; 102–52°W and 30–50°N) to summarize regional differences in the blocking-heatwave linkages.

3 Results

3.1 Atmospheric blocking

CanESM2 and CanESM5 ensembles agree with ERA-Interim and NCEP-DOE-R2 in terms of historical spatial variability of summer blocking frequency, with more frequent blocking days over the north Pacific, Alaska, and western Canada (BR1 and BR2) than central and eastern Canada (BR3 and BR4) (Fig. 1a). This climatological spatial pattern of summer blocking is well documented over Pacific-North America based on reanalyses and GCM simulations (e.g., Woollings et al. 2018; Davini and D'Andrea 2020). Moreover, the two ensembles and reanalyses show a consistent result in the preferred location for blocking occurrence over higher latitudes (i.e., 60–75°N), based on the poleward shift in the position of the jet stream in summer compared to winter (Woollings et al. 2018). However, compared to reanalyses, CanESM2 and CanESM5 ensembles underestimate summer blocking frequency, particularly in regions BR1 and BR2. This is consistent with previous findings from CMIP5 and CMIP6 (e.g., Woollings et al. 2018; Davini and D'Andrea 2020). There are 29 and 25 blocking days of ERA-Interim and 24 and 21 days of NCEP-DOE-R2 versus 15 and 13 days of CanESM2 and 13 and 15 days of CanESM5 on average per summer over BR1 and BR2 (Fig. 1c). This underestimation is also present in CanESM2 in central and eastern Canada (BR3 and BR4); compared to NCEP-DOE-R2, CanESM2 underestimates blocking frequency by -55% at BR3 and 16% at BR4. However, CanESM5 shows good agreement with the reanalyses for summer blocking frequency in these two regions. This may be due to the improved ability of CanESM5 to reproduce features of the large-scale atmospheric circulation. For example, Swart et al. (2019) found improvements in the representation of the 3-D distribution of northward winds, surface zonal winds, sea-ice volume and seasonal cycle, and sea-level pressure, but no significant improvement in 3-D zonal winds, sea-surface temperature, and 3-D geopotential height. Systematic misplacement of the blocking activity from the Alaska toward the North American continent is also shown from both CanESMs. This discrepancy is generally seen in CMIP5 and CMIP6 models and is associated with the overestimation of the Pacific Jet stream speeds and extensions far toward the North Pole (Anstey et al. 2013; Pithan et al. 2016; Davini and D'Andrea 2020).
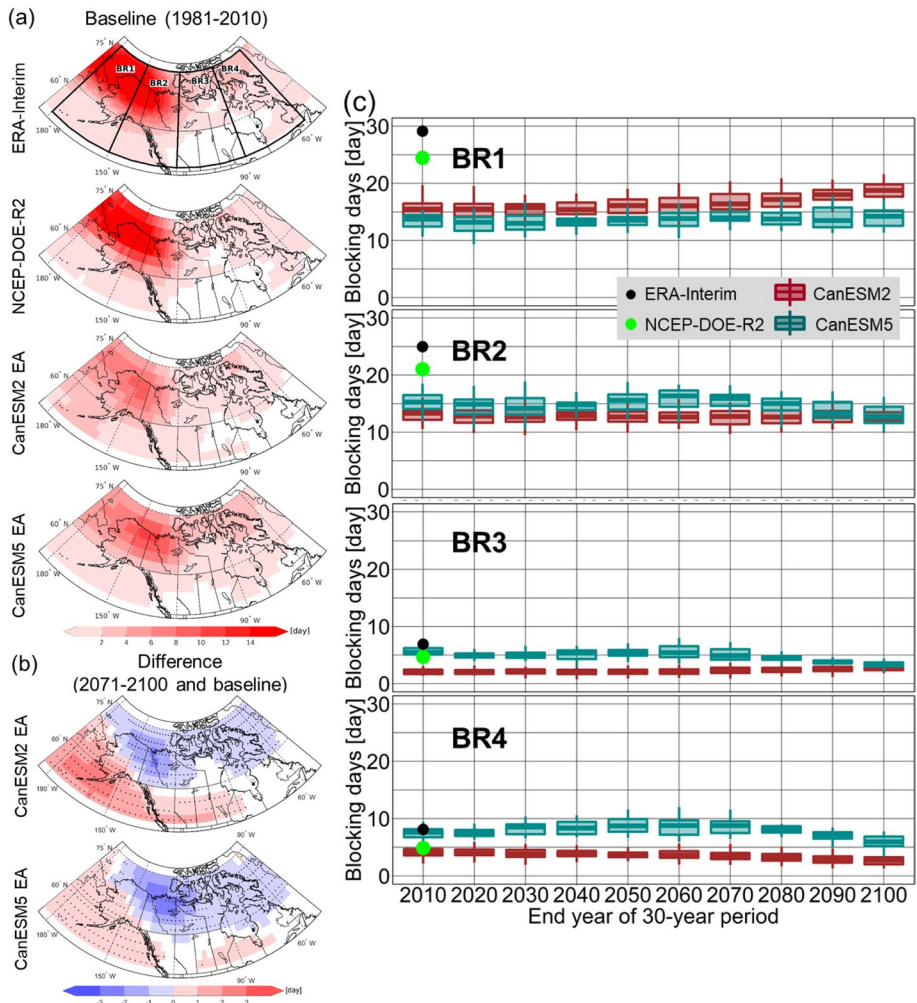
Fig. 1 **a** Two-dimensional summer blocking days of ERA-Interim, NCEP-DOE-R2, and CanESM2 and CanESM5 ensemble averages (EAs) over the Pacific-North America for 1981–2010 baseline, and **b** projected changes of CanESM2 and CanESM5 EAs for 2071–2100 relative to the baseline. Grid points are marked by black dots when ensembles between the baseline and future period are statistically significant based on the two-sample t-test at 10% significance level. **c** Percentages of blocking days in four blocking regions (BR1 to BR4) of ERA-Interim (black dots), NCEP-DOE-R2 (green dots), CanESM2 ensemble (red box-plot), and CanESM5 ensemble (blue box-plot) for the baseline, and projections of the ensembles for future 30-year periods to 2071–2100. The four blocking regions are presented in the first panel of (**a**)

The two ensembles generally project a consistent spatial pattern of changes in summer blocking days. Increases are projected over the Pacific Ocean and in some parts of southern Canada (BR1), while decreases are projected in northern North America and adjacent oceans (BR2 and BR4). However, opposite changes are projected over BR3. Here, CanESM2 projects an increase in blocking days, whereas CanESM5 projects a decrease relative to their baseline levels. While changes in mean blocking frequency may be statistically significant by the end of the twenty-first century, the magnitude of projected changes

are generally small relative to internal variability (Fig. 1c). The largest absolute increase (+ 0.40 day (+ 2.4%)/decade) is projected by CanESM2 ensemble at BR1, while the largest absolute decrease (− 0.27 day (− 1.7%) /decade) is shown by CanESM5 at BR2. In general, results from CanESM5 are in better agreement with previous findings from CMIP5 and CMIP6 multi-model ensembles (Woollings et al. 2018; Davini and D'Andrea 2020). In these studies, it is suggested that warming leads to a poleward shift in the jet stream and Hadley circulation and an attendant decrease in summer blocking frequency, while the signal over the Pacific area is less clear and robust (compared to Greenland) from both CMIP5 and CMIP6 models (Davini and D'Andrea 2020).

3.2 Heatwave events

The spatial variability in summer heatwave frequency simulated by CanESM2 and CanESM5 is generally consistent with the ERA-Interim and NCEP-DOE-R2 reanalyses (Fig. 2a). Inter-ensemble agreement in the spatial pattern of climatological heatwave frequency is high (spatial correlation of 0.84), with slightly lower agreement with the reanalyses (spatial correlation of 0.58 between both ensembles and NCEP-DOE-R2). This suggests that the surface response of the two models to persistence of synoptic-scale atmospheric circulation anomalies and land–atmosphere feedbacks is reasonable (Diro and Sushama 2017). Furthermore, results are in agreement with those reported by Diro and Sushama (2017) in their analysis of heatwaves based on a gridded observation dataset developed using in situ station records.

Under the stationary hot day definition, the two ensembles show significant increases in heatwave days over all regions of North America as the future projection horizon increases from the baseline (Fig. 2c). These increases are due to background warming in response to future emissions and the time-invariant hot day threshold, which is determined from the historical baseline period. CanESM5 projects larger increases in the frequency of heatwave days than does CanESM2 (Fig. 2c), in part because CanESM5 has a higher climate sensitivity than CanESM2 and also because of differences in emissions between the SSP5 8.5 and RCP 8.5 scenarios (Swart et al. 2019).

Under the nonstationary hot day definition, the two ensembles both project small changes in heatwave frequency over North America by the end of the twenty-first century (Fig. 2b). Climatologically, the average number of hot days per summer remains constant over time as the threshold used to define a hot day is calculated separately for each future period. Therefore, a possible way for the number of heatwaves to increase is for the persistence of heat wave days to increase. While changes are statistically significant at some grid points (Fig. 2b), results are not field significant. Furthermore, changes in regional averages over the four regions of North America are not significant (Fig. 2c).

3.3 Linkage between blocking and heatwaves

It should be noted before discussing the blocking-heatwave linkage that blocking cores and associated high-pressure anomalies dominate in the northern parts of blocking regions (higher than 60°N) (Fig. 1a). For the 1981–2010 period, ERA-Interim and NCEP-DOE-R2 display statistically significant connections (tested, as before, by bootstrap resampling at a 10% significance level) between blocking and above-normal heatwave frequency in the northern parts of blocking regions where the blocking cores are dominant, as well as their eastern and/or western sides (Fig. 3a for blocking events at selected regions BR2 and BR3).
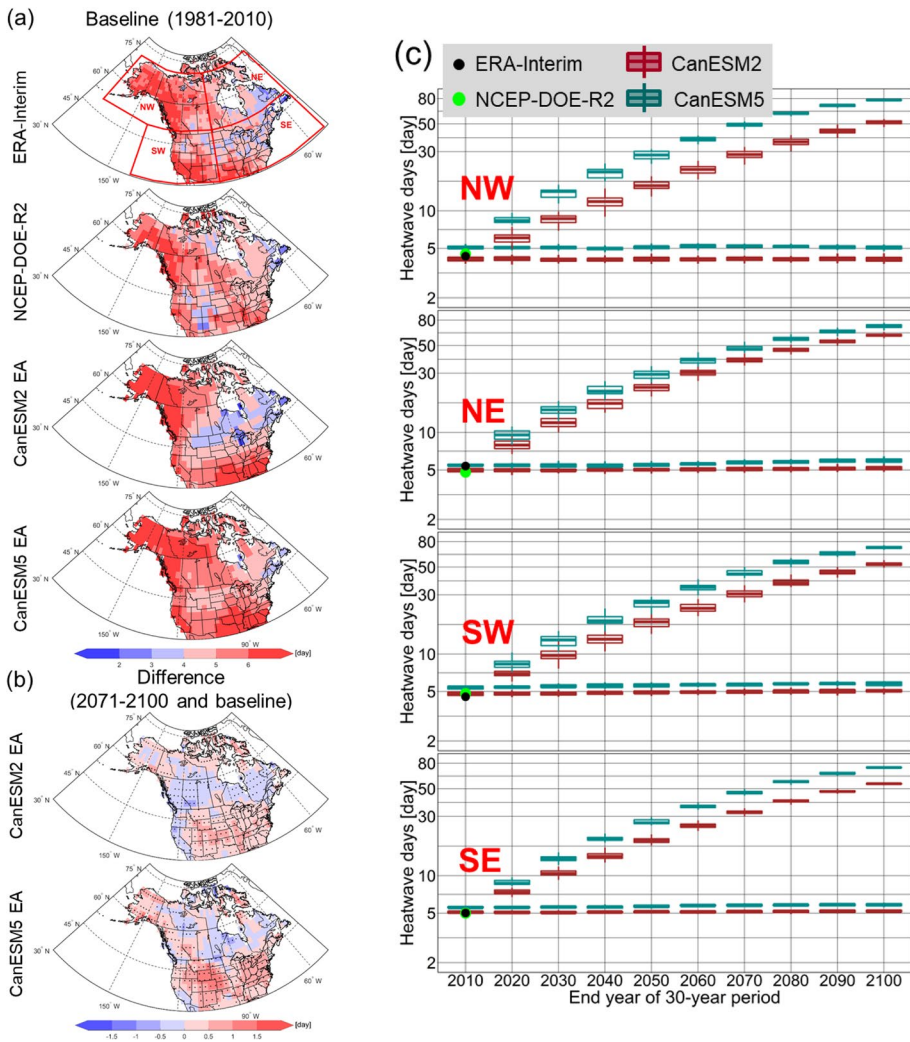
Fig. 2 **a** Summer heatwave days of ERA-Interim, NCEP-DOE-R2, and CanESM2 and CanESM5 ensemble averages (EAs) over North America for 1981–2010 baseline, and **b** projected changes of CanESM2 and CanESM5 EAs under the nonstationary threshold condition for 2071–2100 relative to the baseline. Grid points are marked by black dots when ensembles between the baseline and future period are statistically significant based on the two-sample *t*-test at 10% significant level. **c** Regional averages of heatwave days for ERA-Interim (black dots), NCEP-DOE-R2 (green dots), CanESM2 ensemble (red box-plot), and CanESM5 ensemble (blue box-plot) at the four regions of North America (NW, NE, SW, and SE) for the baseline, and projections of the two ensembles for future 30-year periods. Unfilled and filled box-plots represent stationary and nonstationary hot day threshold definitions. The four regions are presented in the first panel of (**a**)

In particular, based on the reanalyses, about 76% of heatwave events in the NW region occur at the same time as a co-located blocking event over northern North America. Meanwhile, the reanalyses show a statistically significant relationship between blocking and below-normal heatwave frequency at remote locations on the southeastern and/or southern flanks away from the blocking cores (i.e., the northern parts of the blocking regions). These
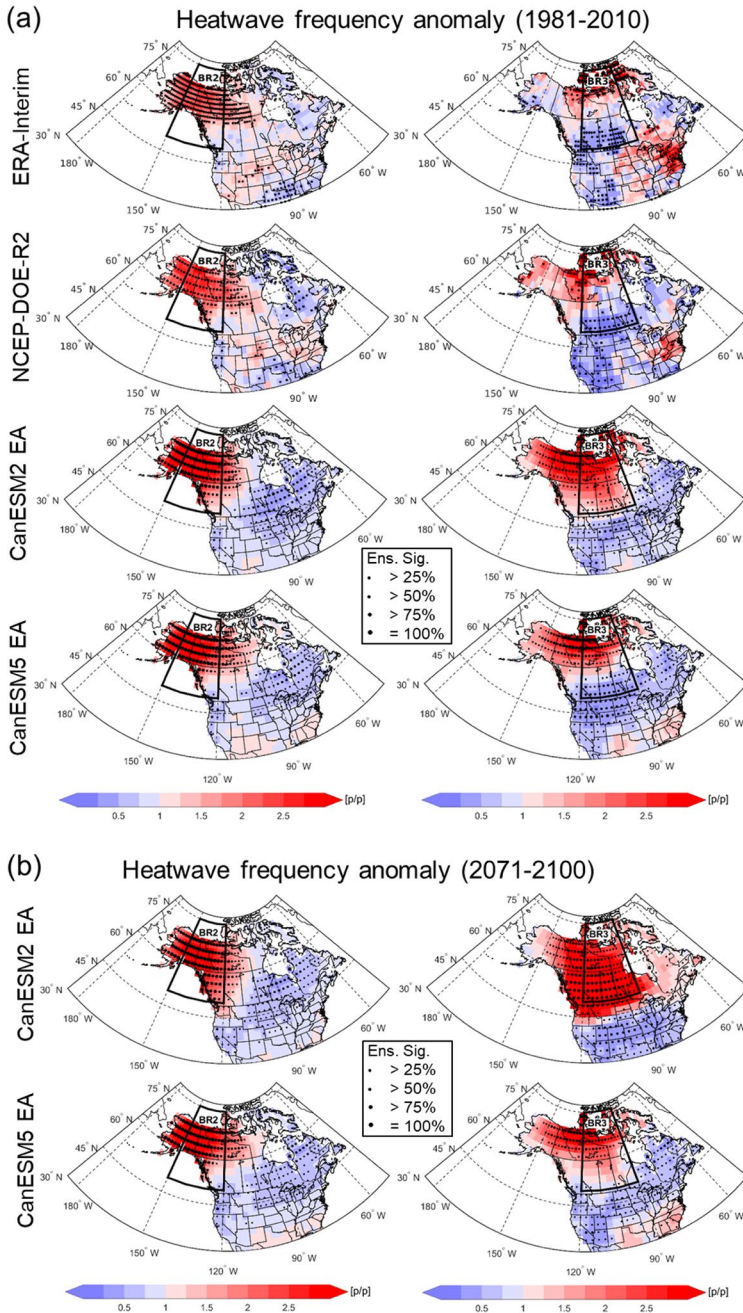
Fig. 3 a Summer heatwave frequency anomaly of ERA-Interim, NCEP-DOE-R2, and CanESM2 and CanESM5 ensemble averages (EAs) over North America when blocking occurs in BR2 (first column) and BR3 (second column) for 1981–2010 baseline as well as **b** those of CanESM2 and CanESM5 EAs for 2071–2100 period. Black dots of ERA-Interim and NCEP-DOE-R2 represent statistical significance at the 10% significant level tested by bootstrap approach. Larger dot size of CanESM2 and CanESM5 ensembles represents larger number of ensemble members yield statistical significance (percentages of the number are defined in the legend)

warm/cold temperature anomalies are mainly due to the location (and extent) of the blocking events and their changes from warm to cold seasons (Wazneh et al. 2021), while cold air advection anomalies on the eastern-side and downstream (i.e., clockwise) from anti-cyclonic blocking episodes could result in the blow-normal frequency anomalies (Pfahl and Wernli 2012; Whan et al. 2016).

The two ensembles generally agree with the two reanalyses in terms of the spatial patterns of the blocking-heatwave linkage, although they overestimate the above-normal heatwave frequency in the NW region during blocking occurring from BR2 to BR4 (Fig. 4). CanESM2 overestimates more than CanESM5, particularly on the southern flanks away from blocking cores (Fig. 3a). Overestimation by the two models may be partly due to over-representation of positive surface radiation anomalies with clear-sky conditions and/or warm temperature advection from the south/east flanks of the blocking events, with other contributing factors including different model configurations and coupling strategies (Swart et al. 2019). The two models also overestimate below-normal heatwave frequency at remote locations on the eastern and southern flanks away from the blocking cores, possibly due to over-representation of negative temperature advection anomalies during blocking events as described in the following section and from potential problems in reproducing meridional wind and storm track features at the east side of the blocking events (Poan et al. 2018). Warm anomalies patterns in eastern Canada have a weak linkage with blocking located over the BR3 or BR4 region, but rather from eastern oceanic areas and/or the Greenland sea (Pfahl and Wernli 2012; Wazneh et al. 2021). Consequently, the two reanalyses generally show insignificant or weak positive linkages between heatwaves of eastern Canada and blocking of B3 and B4, while the CanESM ensembles tend to overestimate the linkages over the baseline period.

Investigation of changes in the blocking-heatwave linkage with climate change is difficult when using the stationary hot day definition due to the significant increase in future heatwave frequency in a warming climate (Fig. 2c). Under the nonstationary hot day threshold, CanESM5 generally simulates similar behavior in the baseline and future periods for both the spatial patterns and regional averages of heatwave frequency anomalies on blocking days (Figs. 3b and 4). This is consistent with the finding for the Euro-Atlantic sector that blocking will continue to play an important role in the development of summer heatwaves in the future under the nonstationary threshold condition (Brunner et al. 2018). CanESM2 also projects the persistence of the baseline behavior into the future period for the blocking-heatwave linkage; however, it suggests large increases in regional averages of the linkage between blocking in BR3 and above-normal heatwave frequency in the NW, NE, and SW regions (Fig. 4). Notably, this is the region where blocking frequency in CanESM2 is significantly negatively biased in the baseline period (by -55% compared to NCEP-DOE-R2). These large increases in CanESM2 are due to increases in the area of above-normal heatwave frequency over middle to northern latitude regions ($>45°$N) for the future period (Fig. 3b) relative to the baseline.

3.4 Atmosphere circulation and surface variables

Compared with the reanalyses, the two climate models simulate similar spatial patterns of positive anomalies of net surface heat flux during blocking over the northern parts of the blocking regions (i.e., the preferred locations for blocking occurrence in Fig. 1a), as well as their eastern and western sides (Fig. 5a). This agreement indicates that the two models reproduce positive surface radiation anomalies resulting from anti-cyclonic high-pressure
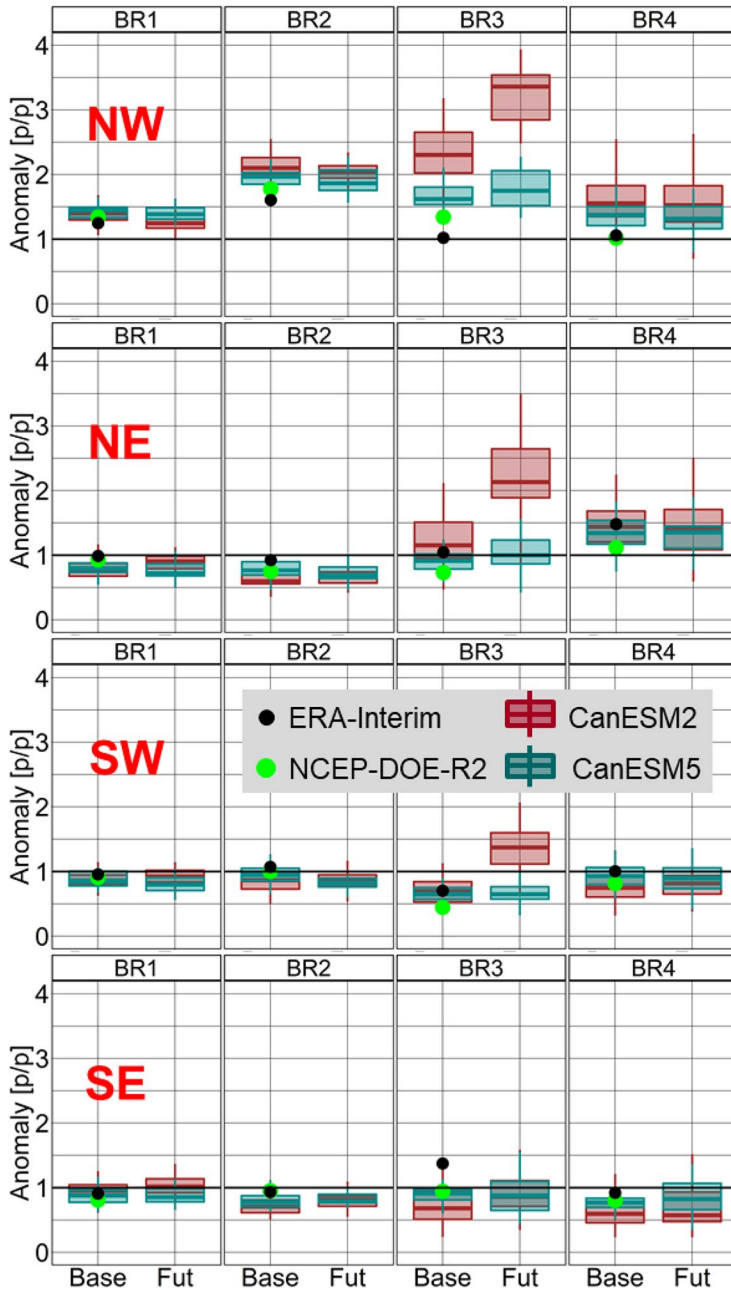
Fig. 4 Regional averages of the heatwave frequency anomaly of ERA-Interim (black dots), NCEP-DOE-R2 (green dots), CanESM2 ensemble (red box-plot), and CanESM5 ensemble (blue box-plot) in the four regions of North America when blocking occurs in regions BR1-BR4 for the baseline, and projections of the two ensembles for 2071–2100 future period
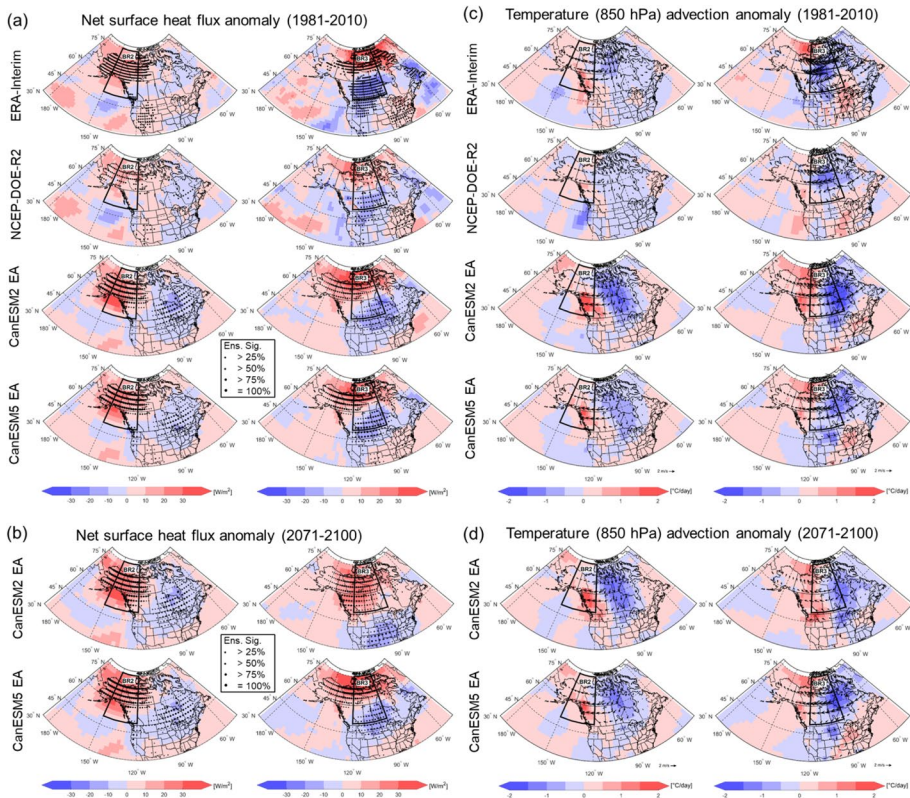
Fig. 5 a Net surface heat flux anomaly and **c** temperature advection anomaly (850 hPa) with wind vector anomaly (arrows over North American grid points) of ERA-Interim, NCEP-DOE-R2, and CanESM2 and CanESM5 ensemble averages (EAs) when blocking occurs in BR2 and BR3 for 1981–2010 baseline, and **b, d** those of CanESM2 and CanESM5 EAs for 2071–2100 future period. Black dots over North American grid points in (**a**) and (**c**) of ERA-Interim and NCEP-DOE-R2 represent statistical significance at the 10% significant level tested by bootstrap approach. Larger dot size of CanESM2 and CanESM5 ensembles represents larger number of ensemble members yield statistical significance (percentages of the number are defined in the legend)

and clear-sky conditions during blocking, particularly in the blocking core and surrounding areas (Pfahl and Wernli 2012). The positive heat flux anomaly is spatially coincident with the above-normal heatwave frequency for each ensemble and reanalysis (Fig. 3a), indicating that surface radiation anomalies during blocking are the main driver of northern North American heatwaves. In addition, diabatic fluxes from sensible heat can also contribute to summer heatwave as deficit of precipitation reduces the evaporation rate and its associated surface cooling. The coupling with soil moisture may also be important. In particular, the positive anomaly of solar radiation that amplifies surface evaporation and the negative anomaly of precipitation associated with blocking causes a gradual depletion of soil moisture, which can result in larger sensible heat fluxes from the surface into the atmosphere (Pfahl and Wernli 2012). Meanwhile, the two ensembles agree with the two reanalyses in terms of negative heat flux anomalies at remote locations along the eastern and southern flanks of the blocking regions. The negative heat flux anomaly is spatially coincident with below-normal heatwave frequency for each ensemble and reanalysis, implying that the

negative anomalies can, along with cold air advection, contribute to below-normal heat-wave frequency.

The two models simulate similar spatial patterns of 850 hPa temperature advection anomalies as the two reanalyses over North America (Fig. 5c). In particular, strong negative temperature advection anomalies are found on the eastern and southern flanks of the blocking cores, due to northerly and/or north-easterly wind anomalies that result from anomalous clockwise anti-cyclonic circulation. This spatial pattern of negative temperature advection anomalies over North America during blocking is in line with findings over Europe (e.g., Trigo et al. 2004; Sousa et al. 2018). Below-normal heatwave frequency at remote eastern and southern regions away from blocking cores (Fig. 3a) can be explained by the negative temperature advection anomalies. Meanwhile, the two climate models and the reanalyses display positive temperature advection anomalies on the southwestern and western regions away from the blocking cores. These are driven by southerly wind anomalies associated with anomalous anti-cyclonic circulation during blocking and they result in above-normal heatwave frequency in those regions. However, CanESM2, CanESM5, and the reanalyses show some regional-scale disagreements for the temperature advection and wind anomalies, and the disagreements lead to the differences in the heatwave frequency anomalies. Specifically, the two climate models yield stronger negative temperature advection anomalies than do the reanalyses at eastern flanks of the blocking regions; this leads to overestimation of below-normal heatwave frequency. Meanwhile, the two ensembles yield stronger positive temperature advection anomalies than the reanalyses along the southern and western flanks of blocking in central Canada (BR3); this leads to overestimation of above-normal heatwave frequency.

For 1000–500 hPa geopotential thickness, CanESM2 and CanESM5 ensembles and reanalyses show positive anomalies along the northern areas of the blocking regions, as well as their eastern and western flanks, but negative anomalies at remote southern and eastern locations away from the blocking cores (Fig. 6a). Therefore, for each ensemble and reanalysis, the positive thickness anomaly (lighter and warmer air-mass than climatology) is spatially consistent with above-normal heatwave frequency and positive heat flux anomaly at the blocking core and surrounding areas. Meanwhile, the negative thickness anomaly also shows spatial agreement with below-normal heatwave frequency and negative temperature advection anomaly at remote eastern and southern locations away from the blocking core. The two ensembles display similar spatial patterns as the reanalyses in terms of negative anomalies of surface precipitation at the northern areas of the blocking regions but positive anomalies at southern areas of the blocking regions, as well as remote eastern locations away from the blocking cores, although the anomalies are less pronounced in the two ensembles compared to ERA-Interim (Fig. 6c). This indicates that the positive and negative anomalies of surface precipitation have relationships with the below- and above-normal heatwave frequency, respectively (Fig. 3a).

In the 2071–2100 period, CanESM5 projects similar spatial patterns of temperature advection and net surface heat flux anomalies during blocking as in the baseline period (Figs. 5b and d). Similar spatial behavior in the two variables supports similar spatial patterns in the linkage between blocking and heatwave frequency anomalies of CanESM5 under the nonstationary threshold condition in the two periods (Fig. 3). However, CanESM2 projects an increase in positive net heat flux anomalies at southern parts of blocking in region BR3. This leads to overestimation of above-normal heatwave frequency as shown in Figs. 3b and 4. CanESM2 also projects an increase in positive temperature advection anomalies at the southern flank of blocking region BR3, which is driven by southerly wind anomalies and contributes to the increase in future heatwave frequency
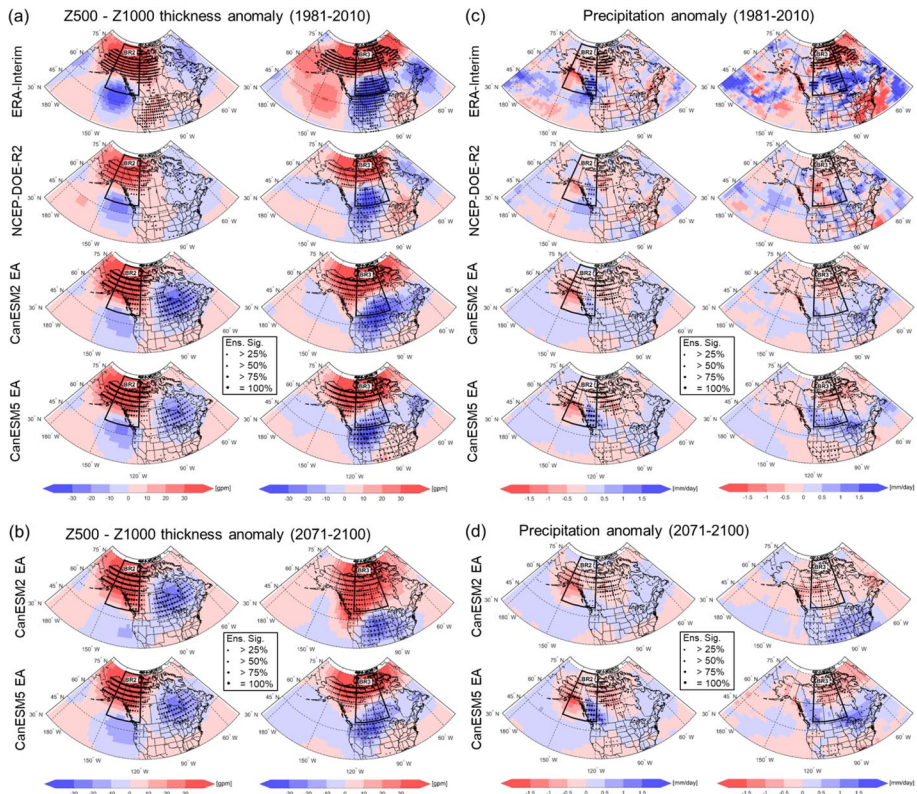
Fig. 6 **a**, **c** 1000–500 hPa geopotential thickness and surface precipitation anomaly of ERA-Interim, NCEP-DOE-R2, and CanESM2 and CanESM5 ensemble averages (EAs) when blocking occurs in BR2 and BR3for 1981–2010 baseline period, and **b**, **d** those of CanESM2 and CanESM5 EAs for 2071–2100 future period. Black dots of ERA-Interim and NCEP-DOE-R2 represent statistical significance at the 10% significant level tested by bootstrap approach. Larger dot size of CanESM2 and CanESM5 ensembles represents larger number of ensemble members yield statistical significance (percentages of the number are defined in the legend)

anomalies. Meanwhile, CanESM5 projects similar spatial patterns of geopotential thickness and precipitation anomalies during blocking in the 2071–2100 and baseline periods (Figs. 6b and d), again supporting the similar spatial patterns in the blocking-heatwave linkage in the two periods. CanESM2, however, projects an increase in geopotential thickness anomalies as well as a decrease in precipitation amount anomalies at the southern parts of the blocking cores in BR3; this also supports the large increases in future above-normal heatwave frequency simulated by CanESM2 during the blocking events.

4 Summary and discussion

The goals of this study are to elucidate the climatological relationships between blocking and summer (June–August) heatwaves over North America, which have been rarely studied before, using two reanalysis datasets (ERA-Interim and NCEP-DOE-R2), and to evaluate the ability of two generations of Canadian Earth System Models (i.e., CanESM2

and CanESM5) to replicate the observed relationships. Furthermore, this study attempts to improve understanding of coincident and remote relationships between blocking and heatwaves using relevant atmosphere circulation and surface variables, including surface heat fluxes, temperature advection, and surface precipitation. Finally, changes in blocking-heatwave linkages in a future warming climate, which have been studied over the Euro-Atlantic sector (e.g., Brunner et al. 2018; Schaller et al. 2018), are evaluated over the North America for the first time.

The comparisons between the two climate models and reanalyses for the 1981–2010 baseline period show that summer high latitude blocking occurs more frequently over the north Pacific, Alaska, and western Canada than central and eastern Canada, as well as at high latitudes (60–70°N) with a systematic misplacement of the two ensembles for the blocking activity from the Alaska toward the North American continent. The two models, however, underestimate summer blocking frequency over those regions (on average by -37% for CanESM2 and -36% for CanESM5 relative to NCEP-DOE-R2), while CanESM2 ensemble also underestimates the frequency in central and eastern Canada (by -36% relative to NCEP-DOE-R2). Underestimation by the two climate models is in line with previous findings based on reanalyses and CMIP5 and CMIP6 GCMs (e.g., Woollings et al. 2018; Davini and D'Andrea 2020). The two climate models and reanalyses generally agree in terms of spatial variability of summer heatwave frequency, for example showing larger values over western and southeastern North America, which is also consistent with results based on a gridded observation dataset (Diro and Sushama 2017). The two climate models and reanalyses generally agree in terms of blocking-heatwave relationships, with above-normal heatwave frequency at co-located blocking cores and surroundings areas (i.e., high-latitudes 60–70°N), but below-normal heatwave frequency occurring at remote locations along the southeastern and/or southern flanks away from the blocking cores. Positive heat flux anomalies at blocking cores and surroundings due to high-pressure system, and negative temperature advection anomalies at remote eastern and southern locations due to northerly/easterly wind anomalies during blocking, result in the above-normal and below-normal heatwave frequencies, respectively.

Projected changes in summer blocking frequency from the 1981–2010 baseline period to 2071–2100 in the two climate models are relatively small compared to internal variability, with the range of absolute changes ranging from $+0.40$ day ($+2.4\%$) to -0.27 day (-1.7%) per decade (Fig. 1c). Projections from CanESM5 are generally in better agreement than CanESM2 with previous findings (Woollings et al. 2018) that show a poleward-shifted jet-stream and Hadley circulation in a warming climate leading to decreases in summer blocking frequency. Under nonstationary threshold definition, the two ensembles project very small changes in heatwave days over North America (smaller than $\pm 1\%$/decade in regional averages at four North American sub-regions). CanESM5 generally simulates similar behavior in the baseline and 2071–2100 periods for spatial distribution as well as regional averages of the blocking-heatwave linkage under the nonstationary threshold condition. This is consistent with the finding over Euro-Atlantic sector that blocking will continue to play an important role in the development of summer heatwaves in the future under the nonstationary threshold condition (Brunner et al. 2018). However, CanESM2 simulates large increases in the linkage between blocking and above-normal heatwave frequency over northern and southwestern regions of North America during blocking events in central Canada. These changes in the blocking-heatwave linkage simulated by CanESM2 can be explained by changes in anomalies of surface heat flux, temperature advection, and surface precipitation during blocking events. RCP 8.5/SSP5 8.5 is recently considered unrealistically high-emission scenarios (e.g., Ritchie and Dowlatabadi 2017; Hausfather and Peters

2020). The main features in the projected linkages between blocking and summer heatwave under a lower emission scenario could be in the range of the projections of this study, given the monotonic changes in the frequencies of blocking and summer heatwaves in response to increase in emission concentrations.

Relative to CanESM2, CanESM5 is better able to reproduce observed summer blocking frequency over central and eastern Canada, as well as the blocking-heatwave linkage over northwest North America during blocking events in Alaska and western and central Canada (Fig. 4). This is likely due to overall improvements of CanESM5 over CanESM2 in simulating 3-D distribution of northward winds, surface zonal winds, sea-ice volume and seasonal cycle, and sea-level pressure, while no significant improvement in 3-D zonal wind, sea-surface temperature, and 3-D geopotential height (Swart et al. 2019). Therefore, future blocking-heatwave linkages projected by CanESM5 could be more reliable, although CanESM2 also makes similar projections, with the exception of the linkage during blocking events occurring over central Canada, which are significantly underestimated (by − 55%) compared to the reanalyses. However, better projections of blocking-heatwave relationships, particularly over northern North America, which has strong positive relationships with blocking activities, may require climate models that have finer resolution and a better physical parameterization for both dynamics and thermodynamics processes, sea surface temperature, orographic drag, sea-ice features, etc. in order to reduce negative biases in blocking frequency (Pithan et al. 2016; Sousa et al. 2018; Davini and D'Andrea 2020).

The approach used in this study evaluates positive linkages between blocking of BR1 and BR2 and heatwaves of NW and between blocking of BR4 and heatwaves of NE, while negative linkages between blocking of BR2 and heatwaves of NE, between blocking of BR3 and heatwaves of SW, and between blocking of BR4 and heatwaves of SW and SE (Fig. 4). However, further assessments should be needed to better understand the mechanisms driving summer heatwaves and how these mechanisms and extremes will be affected by climate change over North America. In particular, summer heatwave characteristics are not only affected by large scale features that is focused in this study but also by regional scale factors such as sensible and latent heat fluxes at the surface, vertical advection, and diabatic heating (Sousa et al. 2018). Continued research is needed to evaluate the impacts of blocking on other climate extremes such as drought and extreme precipitation over North America using global and regional climate models under different future emission scenarios. This study focused on the impacts of high latitude blocking that diverts the main westerly flow on summer heatwaves; however, subtropical ridges, which are known to have impacts on European heatwave (Sousa et al. 2018) and weak blocking events and warm anomalies in eastern Canada (Pfhal and Wernli 2012), are not covered in this study. Moreover, further investigations are needed to understand the relationships between blocking and hot temperature extremes in the other seasons.

References

Alizadeh MR, Abatzoglou JT, Adamowski JF, Prestemon JP, Chittoori B, AkbariAsanjan A, Sadegh M (2022) Increasing heat stress inequality in a warming climate. Earth's Future 10:e2021EF002488. https://doi.org/10.1029/2021EF002488

Anstey JA, Davini P, Gray LJ, Woollings TJ, Butchart N, Cagnazzo C, Christiansen B, Hardiman SC, Osprey SM, Yang S (2013) Multi-model analysis of Northern Hemisphere winter blocking: model biases and the role of resolution. J Geophys Res Atmos 118:3956–3971

Arora VK, Scinocca JF, Boer GJ, Christian JR, Denman KL, Flato GM, Kharin VV, Lee WG, Merryfield WJ (2011) Carbon emission limits required to satisfy future representative concentration pathways of greenhouse gases. Geophys Res Lett 38:L05805. https://doi.org/10.1029/2010GL046270

Barriopedro D, García-Herrera R, Trigo RM (2010) Application of blocking diagnosis methods to general circulation models. Part I: A Novel Detect Scheme Clim Dyn 35(7):1373–1391

Berckmans J, Woollings T, Demory ME, Vidale PL, Roberts M (2013) Atmospheric blocking in a high resolution climate model: Influences of mean state, orography and eddy forcing. Atmos Sci Let 14:34–40

Black E, Blackburn M, Harrison G, Hoskins B, Methven J (2004) Factors contributing to the summer 2003 European heatwave. Weather 59(8):217–223. https://rmets.onlinelibrary.wiley.com/doi/abs/10.1256/wea.74.04

Brunner L, Schaller N, Anstey J, Sillmann J, Steiner AK (2018) Dependence of present and future European temperature extremes on the location of atmospheric blocking. Geophys Res Lett 45(12):6311–6320

Davini P, D'Andrea F (2020) From CMIP3 to CMIP6: Northern Hemisphere atmospheric blocking simulation in present and future climate. J Clim 33(23):10021–10038

Davini P, Cagnazzo C, Gualdi S, Navarra A (2012) Bidimensional diagnostics, variability, and trends of Northern Hemisphere blocking. J Clim 25(19):6496–6509

Dee DP et al (2011) The ERA-Interim reanalysis: configuration and performance of the data assimilation system. Q J R Meteorol Soc 137(656):553–597

Diro GT, Sushama L (2017) The role of soil moisture–atmosphere interaction on future hot spells over North America as simulated by the Canadian regional climate model (CRCM5). J Clim 30(13):5041–5058

Dong L, Mitra C, Greer S, Burt E (2018) The dynamical linkage of atmospheric blocking to drought, heatwave and urban heat island in Southeastern US: a multi-scale case study. Atmosphere 9(1):33

Dosio A, Mentaschi L, Fischer EM, Wyser K (2018) Extreme heat waves under 1.5 C and 2 C global warming. Envir Res Lett 13(5):054006

Efron B, Tibshirani RJ (1994) An introduction to the bootstrap. CRC Press, New York

Eyring V, Bony S, Meehl GA, Senior CA, Stevens B, Stouffer RJ, Taylor KE (2016) Overview of the Coupled Model Intercomparison Project Phase 6 (CMIP6) experimental design and organization. Geosci Model Dev 9:1937–1958

Fischer EM, Knutti R (2015) Anthropogenic contribution to global occurrence of heavy-precipitation and high-temperature extremes. Nat Clim Change 5(6):560–564

Fischer EM, Seneviratne SI, Vidale PL, Lüthi D, Schär C (2007) Soil moisture–atmosphere interactions during the 2003 European summer heat wave. J Clim 20(20):5081–5099

Fyfe JC, Derksen C, Mudryk L, Flato GM, Santer BD, Swart NC, Molotch NP, Zhang X, Wan H, Arora VK, Sciocca J, Jiao Y (2017) Large near-term projected snowpack loss over the western United States. Nat Commun 8:14996. https://doi.org/10.1038/ncomms14996

García-Herrera R, Díaz J, Trigo RM, Luterbacher J, Fischer EM (2010) A review of the European summer heat wave of 2003. Crit Rev Environ Sci Technol 40(4):267–306

Hausfather Z, Peters GP (2020) Emissions-the 'business as usual' story is misleading. Nature 577(7792):618–621

Hersbach H et al (2020) The ERA5 global reanalysis. Q J R Meteorol Soc 146(730):1999–2049

IPCC (2013) Climate Change 2013. The physical science basis. Contribution of Working Group I to the Fifth Assessment Report of the Intergovernmental Panel on Climate Change [Stocker TF, Qin D, Plattner G-K, Tignor M, Allen SK, Boschung J, Nauels A, Xia Y, Bex V, and Midgley PM (eds.)], Cambridge University Press, Cambridge, United Kingdom and New York, NY, USA

Jeong DI, Yu B, Cannon AJ (2021) Links between atmospheric blocking and North American winter cold spells in two generations of Canadian Earth System Model large ensembles. Clim Dyn 57:2217–2231

Kanamitsu M, Ebisuzaki W, Woollen J, Yang SK, Hnilo JJ, Fiorino M, Potter GL (2002) NCEP–DOE AMIP-II reanalysis (R-2). Bull Am Meteorol Soc 83(11):1631–1644

Lee JY, Marotzke J, Bala G, Cao L, Corti S, Dunne JP, Engelbrecht F, Fischer E, Fyfe JC, Jones C, Maycock A, Mutemi J, Ndiaye O, Panickal S, Zhou T (2021) Future global climate: scenario-based projections and near-term information. In: Climate Change 2021: The Physical Science Basis. Contribution of Working Group I to the Sixth Assessment Report of the Intergovernmental Panel on Climate Change [Masson-Delmotte V, Zhai P, Pirani A, Connors SL, Péan C, Berger S, Caud N, Chen Y, Goldfarb L, Gomis MI, Huang M, Leitzell K, Lonnoy E, Matthews JBR, Maycock TK, Waterfield T, Yelekçi O, Yu R, Zhou B (eds.)]. Cambridge University Press

Lehtonen I, Karpechko AY (2016) Observed and modeled tropospheric cold anomalies associated with sudden stratospheric warmings. J Geophys Res Atmos 121(4):1591–1610

Li M, Yao Y, Simmonds IH, Luo D, Zhong L, Chen X (2020) Collaborative impact of the NAO and atmospheric blocking on European heatwaves, with a focus on the hot summer of 2018. Envir Res Lett 15:114003

Moss R et al (2010) The next generation of scenarios for climate change research and assessment. Nature 463:747–756

National Climatic Data Center (2001) Billion dollar US weather disasters 1980–2001. http://lwf.ncdc.noaa.gov/oa/reports/billionz.html#LIST

O'Neill BC et al (2014) A new scenario framework for climate change research: the concept of shared socioeconomic pathways. Clim Change 122(3):387–400

Overland JE (2021) Causes of the record-breaking Pacific Northwest heatwave, late June 2021. Atmosphere 12(11):1434. https://doi.org/10.3390/atmos12111434

Pereira SC, Marta-Almeida M, Carvalho AC, Rocha A (2017) Heat wave and cold spell changes in Iberia for a future climate scenario. Int J Climatol 37(15):5192–5205

Peterson TC et al (2013) Monitoring and understanding changes in heat waves, cold waves, floods, and droughts in the United States: state of knowledge. Bull Am Meteorol Soc 94(6):821–834

Pettenuzzo D, Large WG, Pinardi N (2010) On the corrections of ERA-40 surface flux products consistent with the Mediterranean heat and water budgets and the connection between basin surface total heat flux and NAO. J Geophys Res 115:C06022. https://doi.org/10.1029/2009JC005631

Pfahl S, Wernli H (2012) Quantifying the relevance of atmospheric blocking for co-located temperature extremes in the Northern Hemisphere on (sub-)daily time scales. Geophys Res Lett 39:L12807

Pithan F, Shepherd TG, Zappa G, Sandu I (2016) Climate model biases in jet streams, blocking and storm tracks resulting from missing orographic drag. Geophys Res Lett 43:7231–7240

Poan ED, Gachon P, Laprise R, Aider R, Dueymes G (2018) Investigating added value of regional climate modeling in North American winter storm track simulations. Clim Dyn 50:1799–1818

Ritchie J, Dowlatabadi H (2017) Why do climate change scenarios return to coal? Energy 140:1276–1291

Rohrer M, Martius O, Raible CC, Brönnimann S (2020) Sensitivity of blocks and cyclones in ERA5 to spatial resolution and definition. Geophys Res Lett 47:e2019GL085582. https://doi.org/10.1029/2019GL085582

Schaller N, Sillmann J, Anstey J, Fischer EM, Grams CM, Russo S (2018) Influence of blocking on Northern European and Western Russian heatwaves in large climate model ensembles. Envir Res Lett 13(5):054015

Schiemann R et al (2020) Northern Hemisphere blocking simulation in current climate models: evaluating progress from the Climate Model Intercomparison Project Phase 5 to 6 and sensitivity to resolution. Weather Clim Dyn 1(1):277–292

Schulzweida U (2019) CDO User Guide (Version 1.9.6). Max Planck Institute for Meteorology, Hamburg, Germany.

Schwierz C, Croci-Maspoli M, Davies HC (2004) Prespicacious indicators of atmospheric blocking. Geophys Res Lett 31:L06125. https://doi.org/10.1029/2003GL019341

Sejian V, Naqvi SMK, EzejiJeffrey T, Lal L (2012) Environmental stress and amelioration in livestock production. Springer, Berlin

Seneviratne SI et al (2010) Investigating soil moisture–climate interactions in a changing climate: a review. Earth Sci Rev 99(3):125–161

Seneviratne SI, Zhang X, Adnan M, Badi W, Dereczynski C, Di Luca A, Ghosh S, Iskandar I, Kossin J, Lewis S, Otto F, Pinto I, Satoh M, Vicente-Serrano SM, Wehner M, Zhou B (2021) Weather and climate extreme events in a changing climate. In: Climate Change 2021: The Physical Science Basis. Contribution of Working Group I to the Sixth Assessment Report of the Intergovernmental Panel on Climate Change [Masson-Delmotte V, Zhai P, Pirani A, Connors SL, Péan C, Berger S, Caud N, Chen

Y, Goldfarb L, Gomis MI, Huang M, Leitzell K, Lonnoy E, Matthews JBR, Maycock TK, Waterfield T, Yelekçi O, Yu R, Zhou B (eds.)]. Cambridge University Press.

Sousa PM, Trigo RM, Barriopedro D, Soares PM, Santos JA (2018) European temperature responses to blocking and ridge regional patterns. Clim Dyn 50(1–2):457–477

Swart NC et al (2019) The Canadian Earth System Model version 5 (CanESM5. 0.3). Geosci Model Dev 12(11):4823–4873

Taylor KE, Stouffer RJ, Meehl GA (2012) An overview of CMIP5 and the experiment design. Bull Am Meteorol Soc 93(4):485–498

Trigo RM, Trigo IF, DaCamara CC, Osborn TJ (2004) Climate impact of the European winter blocking episodes from the NCEP/NCAR Reanalyses. Clim Dyn 23:17–28

Virgin JG, Fletcher CG, Cole JNS, von Salzen K, Mitovski T (2021) Cloud feedbacks from CanESM2 to CanESM5.0 and their influence on climate sensitivity. Geosci Model Dev 14:5355–5372

Wazneh H, Gachon P, Laprise R, de Vernal A, Tremblay B (2021) Atmospheric blocking events in the North Atlantic: trends and links to climate anomalies and teleconnections. Clim Dyn 56:2199–2221

Whan K, Zwiers F, Sillmann J (2016) The influence of atmospheric blocking on extreme winter minimum temperatures in North America. J Clim 29(12):4361–4381

Woollings T, Barriopedro D, Methven J, Son SW, Martius O, Harvey B, Sillmann J, Lupo AR, Seneviratne S (2018) Blocking and its response to climate change. Curr Clim Change Rep 4(3):287–300

Zappa G, Masato G, Shaffrey L, Woollings T, Hodges K (2014) Linking Northern Hemisphere blocking and storm track biases in the CMIP5 climate models. Geophys Res Lett 41:135–139